Rydberg Excitons in Synthetic Cuprous Oxide (Cu$_2$O)

Stephen A. Lynch,* Chris Hodges, Soumen Mandal, and Wolfgang Langbein
School of Physics and Astronomy, Cardiff University, Cardiff CF24 3AA, United Kingdom.

Ravi P. Singh
Department of Physics, Indian Institute of Science Education and Research (IISER) Bhopal, India.

Liam A. P. Gallagher, Jon D. Pritchett, Danielle Pizzey,
Joshua P. Rogers, Charles S. Adams, and Matthew P. A. Jones
*Joint Quantum Centre Durham-Newcastle, Department of Physics,
Durham University, Durham DH1 3LE, United Kingdom.*
(Dated: 04/08/2021 at 12:21:46)

High-lying Rydberg states of Mott-Wannier excitons are receiving considerable interest due to the possibility of adding long-range interactions to the physics of excitons. Here, we study Rydberg excitation in bulk synthetic cuprous oxide grown by the optical float zone technique and compare the result with natural samples. X-ray characterization confirms both materials are mostly single crystal, and mid-infrared transmission spectroscopy revealed little difference between synthetic and natural material. The synthetic samples show principal quantum numbers up to $n = 10$, exhibit additional absorption lines, plus enhanced spatial broadening and spatial inhomogeneity. Room temperature and cryogenic photoluminescence measurements reveal a significant quantity of copper vacancies in the synthetic material. These measurements provide a route towards achieving high-n excitons in synthetic crystals, opening a route to scalable quantum devices.

I. INTRODUCTION

The study of highly excited Rydberg exciton states facilitates an exciting crossover between two previously siloed disciplines: cold-atom physics and semiconductor quantum optics. The coherent spectroscopy of Rydberg states in gas-phase atomic systems has garnered great recent interest, with applications in the measurement of electromagnetic fields from DC to terahertz frequencies [1, 2], quantum simulation [3] and computation [4], and quantum optics [5]. There is clear interest in observing similar states in semiconductor systems, where half a century of development in state-of-the-art nano-fabrication techniques provide capabilities that go way beyond those available in the gas phase. Cuprous oxide raises the tantalizing prospect of a material where Rydberg atom analogues can be created on-demand in an environment that more naturally lends itself to engineering multiple quantum interactions, and furthermore offers a plausible pathway to scale up. Experiments in high-quality natural crystals have revealed the potential of cuprous oxide but realizing synthetic material with comparable quantum optical properties is a prerequisite for the material to achieve technological traction. In this paper we discuss our progress towards achieving synthetic cuprous oxide single crystals that exhibit high-n excitons.

Single crystal cuprous oxide (Cu$_2$O) was one of the first semiconducting crystals used in electronics [6, 7], and received considerable attention until silicon eventually prevailed as the semiconductor of choice for microelectronic applications. However, it is the unique optical properties that cause it to stand out from other semiconductor crystals. The Cu$_2$O band gap of 2.17 eV is about twice that of silicon, making it suited to complement silicon as a solar cell material [8]. The spectroscopic property of paramount interest to us is its extraordinary excitonic spectrum [9]. Excitons are bound electron and hole quasi-particles that exhibit a series of sharp spectral lines (not unlike the Rydberg series of hydrogen) near the semiconductor band edge. Because the exciton binding energy is typically in the meV range, the exciton lines are mostly observed at cryogenic temperatures. While it is common to observe excitons up to principal quantum numbers of $n = 3$ in conventional compound semiconductors such as GaAs [10], it has long been known that excitons with higher-n can be observed in Cu$_2$O crystals [11]. The Cu$_2$O-exciton system has been used over the last three decades to test for evidence of Bose-Einstein condensation in the solid state [12], due to its forbidden exciton ground state transition.

However, it is the 2014 paper by Kazimierczuk *et al.* reporting excitons with $n = 25$ that has generated renewed interest in this material system [13]. Excitons may be described using a modified Bohr model [14, 15], with the energy level spectrum described by,

$$E_{\mathrm{X}}(n) = -\left(\frac{\mu}{m_0}\right)\frac{1}{\epsilon_r^2}\frac{R_{\mathrm{H}}}{n^2} = -\frac{R_{\mathrm{X}}}{n^2} \quad , \qquad (1)$$

and exciton radius,

$$\langle r_n \rangle = n^2 \left(\frac{m_0}{\mu}\right)\epsilon_r a_{\mathrm{H}} = n^2 a_{\mathrm{X}} \quad . \qquad (2)$$

Here μ is the two-body reduced mass, R_{H} and R_{X} are the hydrogen and exciton Rydberg constants respectively, a_{H}

* LynchSA@cardiff.ac.uk

and a_X are the hydrogen and exciton Bohr radii respectively, and the other symbols have their usual meanings. For the results in [13], the relevant excitonic states give rise to the "yellow" series of transitions between the states of the uppermost valence and lowest conduction bands. Since the band states have the same parity, the excitonic energy levels have P (i.e. orbital angular momentum $l = 1$) symmetry. A narrow quadrupole transition to the dipole-forbidden 1S state is also be observed, and phonon-assisted 1S transitions contribute a substantial background to the spectrum of nP states. The electron and hole effective masses are usually taken to be [16, 17] $m_e = 0.99\ m_0$ and $m_h = 0.58\ m_0$, which gives $\mu = 0.37\ m_0$. There is some discussion over the correct value of ϵ_r to use. The high-frequency relative permittivity value is often quoted as [16] $\epsilon_r(\infty) = 6.46$, which gives $R_X = 120.6$ meV. However, since the ground state 1S exciton is known to have an anomalously large binding energy [18], this value is not used. Instead, researchers use the modified Bohr formula (equation 1) to fit the energies of the higher lying P-excitons, yielding a smaller exciton Rydberg energy of 98.3 meV, which corresponds to $\epsilon_r = 7.2$. In reality the situation is more complicated. When the non-parabolicity of the bands, phonon coupling, and the spin interaction are properly taken into account [18], the adjusted Bohr radius of the exciton is calculated to be $a_X = 1.11$ nm. Kazimierczuk *et al.* use this value together with an average radius $\langle r_n \rangle$ derived from the spherical harmonics of the $n = 25$ P-state wave-functions to predict $\langle r_{25} \rangle = 1.04$ µm. In atomic systems, the large spatial extent of excitonic wave-functions means that interactions between them are dominated by long-range van der Waals forces [19]. Unlike the short-range exchange-type interaction more commonly studied for ground state excitons, such long-range interactions can enable strong non-local [20] optical non-linearities [21, 22] without overlap between the excitonic wave-functions. While widely studied in atomic systems [5], the first hints of such long-range interactions in crystals were observed in Kazimierczuk *et al.* [13], with subsequent confirmation via pump-probe experiments [23].

So far however, these results [13] have not been reproduced by other groups, due to difficulties in obtaining samples of high quality. Most groups currently report on natural gemstones of various quality (Fig. 1(a)). The highest quality synthetic samples, while reproducible, are inferior to their natural counterparts. The highest principal quantum number measured to date in a synthetic stone is $n = 10$ [24]. Wider availability of the high-quality samples required for the observation of high-n excitons is an essential step towards various quantum-optical devices based on Rydberg excitons [25–28].

Several methods for producing Cu_2O have been reported in the literature. Thin films have been prepared by several deposition methods, including reactive sputtering [29], thermal oxidation [30], electrodeposition [31, 32], melting [33], and metal-organic chemical vapour deposition (MOCVD) [34]. However, the experimental conditions necessary to observe high-n excitons impose severe constraints on the thermal expansion properties of any supporting substrate to prevent strain accumulation in the thin film on cooling to cryogenic temperatures. This is because the large spatial extent of the high-n exciton wave-function should make it particularly sensitive to any distortions to the crystal lattice resulting from macroscopic strain fields [35, 36]. Consequently, we have chosen to pursue a path towards macroscopic single crystal growth using float-zone (FZ) refining, to avoid the thermal strain that would occur on cryogenic cooling if the Cu_2O was bonded to a different substrate. This method has been successfully employed in the past to produce large single crystals [24, 37, 38]. Our method of growth is detailed below and is similar to method used in [38].

II. METHODS

A. Crystal Growth

The starting material was 5 mm diameter copper rod, Puratronic® 99.999% (metals basis) from Alfa Aeser. The Cu_2O feed and seed rods were prepared by thermal oxidation of the copper metal rods at $1100°C$ for approximately 40 hours in air at atmospheric pressure. The oxidized rods were then used to grow the single crystal material in a Crystal Systems Corporation (CSC) optical furnace (model: FZ-T-10000-H-VII-VPM-MII-PC). Localized heating was achieved by bringing the light from four halogen lamps to a joint focus on the sample using four semi-ellipsoidal mirrors. The growth region is isolated from the furnace by a quartz tube allowing the use of different growth atmospheres and pressures- in this work we used air at atmospheric pressure. Single-crystal growth is achieved by melting a feed rod and fusing it to a seed rod, establishing a freely floating molten zone. This floating zone was then scanned up the feed rod at a controlled slow speed of 4.0-7.0 mm/hour, with the feed and seed rods rotating at 20 rpm in opposite directions. This method has the advantage that it doesn't require a crucible, which is critical in this application because molten Cu_2O is known to react with standard crucible materials [37]. Figure 1(b) shows two 5 mm Cu_2O single crystals after FZ growth together with the same gemstone shown in (a), with a perspex lab ruler on the right for scale.

B. Sample Preparation

For characterization, the crystals were cut into 2-3 mm thick disks perpendicular to the cylindrical axis using a diamond saw. The samples were encapsulated in acrylic resin and lapped back to reveal the front surface of the Cu_2O. The uncovered Cu_2O surface was then polished optically flat on a Struers LaboPol-5 lapping machine,
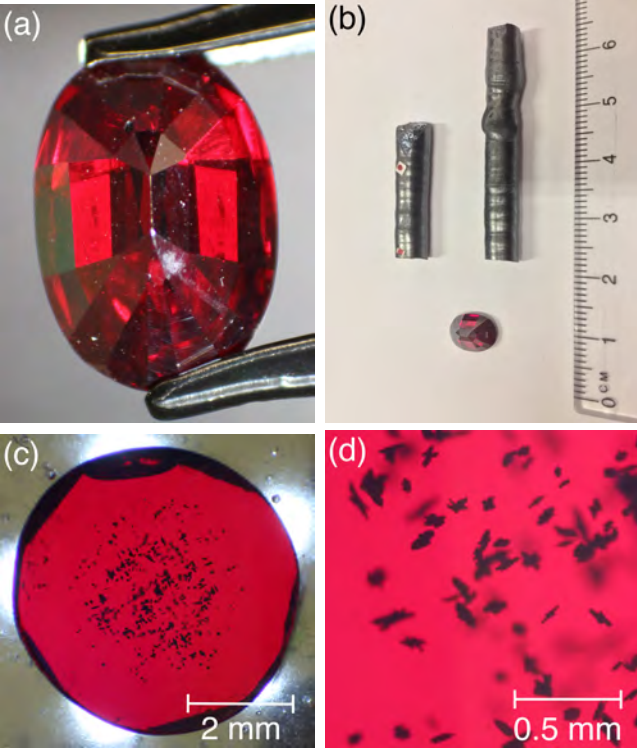
FIG. 1. (a) A commercially available natural cuprite gemstone. (b) Two synthetic single crystals of Cu_2O grown in this work with the same natural gemstone for scale. (c) Backlit slice of optically polished synthetic crystal. (d) Higher magnification optical image of the same slice highlighting the inclusions (dark specs).
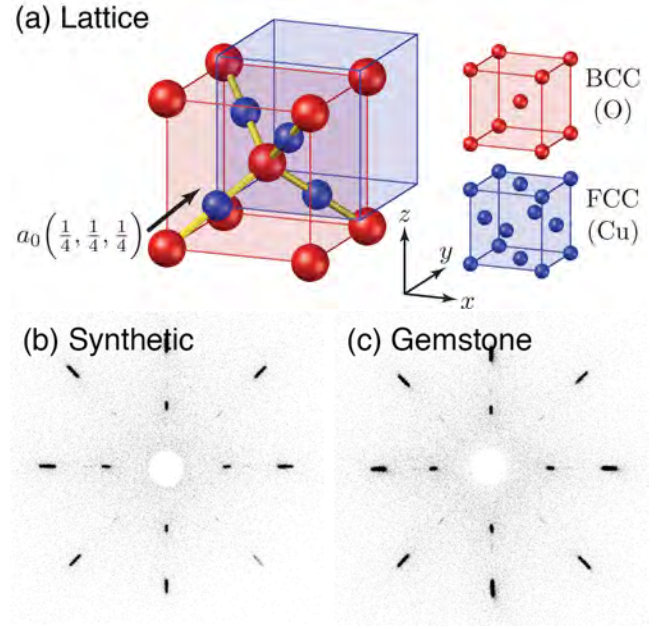

FIG. 2. (a) Interleaved BCC/FCC lattice of Cu_2O. The oxygen (O) atoms are located at the lattice points of the BCC cubic cell, while the copper (Cu) atoms lie at the lattice points of the FCC cubic cell with the same dimensions (a_0). The two cubic cells are offset by $a_0\left(\frac{1}{4},\frac{1}{4},\frac{1}{4}\right)$. Laue spot pattern of both the (b) synthetic and (c) natural material for comparison. The crystals were both aligned so that the incoming beam X-ray beam is orthogonal to the 100 plane $(1\,0\,0)$ crystal plane. These Laue patterns highlight the cubic symmetry and single crystal nature of both samples of Cu_2O material.

employing a 4-step process using Struers consumables. Step 1 was a rough grind of the surface using a MD-Largo disk together with DiaPro Allegro/Largo 9 µm diamond suspension/lubricant for 2 minutes. Step 2 was a rough polish on a Struers DP-DAC satin woven acetate cloth disk together with DiaPro DAC 3 µm diamond suspension/lubricant for a further 5 minutes. Step 3 was a fine polishing step on a DP-NAP cloth together with a 1 µm DiaPro NAP suspension/lubricant for further 15-30 minutes. Step 4 covered the final polishing, where we used a new DP-NAP cloth together with 0.25 µm DiaPro NAP suspension/lubricant. During the final polishing step, the sample was periodically inspected under a stereo-microscope, and this step was repeated until visible surface scratches/digs were removed. The other side of the sample was then lapped and polished according to the same procedure. The final thickness of the polished samples was between 50-100 µm for optical measurements. Thicker samples (2-3 mm), prepared in a similar way, were used for mid-infrared measurements. A typical low-magnification cross-sectional image is shown in figure 1(c), showing homogeneous optically transparent material with the deep red signature color of Cu_2O near the outside of the disk and an increasing concentration of small dark inclusions localized towards the center.

Figure 1(d) shows the same cross-sectional slice captured at greater magnification, highlighting the inclusions towards the center of the disk. These inclusions closely resemble those observed in previous works [37, 39] where they were found to be voids with cupric oxide (CuO) walls.

C. X-ray Analysis

X-ray analysis was performed using a Laue camera. The x-ray source was a tungsten x-ray tube. The back-scattered Laue spot pattern when the $(1\,0\,0)$ crystal plane is aligned perpendicular to the X-ray beam is shown in figure 2(b) and (c) for both synthetic and commercially available natural material respectively. These Laue patterns confirm the single crystal nature of both the synthetic Cu_2O material, and the natural gemstones. Cu_2O has an interleaved cubic lattice. The Cu atoms sit at the lattice points of a face-centered cubic (FCC) cell, while the oxygen atoms are located at the lattice points of a shifted body centered cubic (BCC) lattice [40], as shown in figure 2(a). The expected cubic symmetry of the crystal is clear from the Laue patterns in the bottom of this figure.

D. Visible Spectroscopy

The Rydberg exciton spectrum at 5 K for our synthetic material is shown in Figure 3, along with a corresponding spectrum measured for the natural gemstone material for comparison. The samples were illuminated by
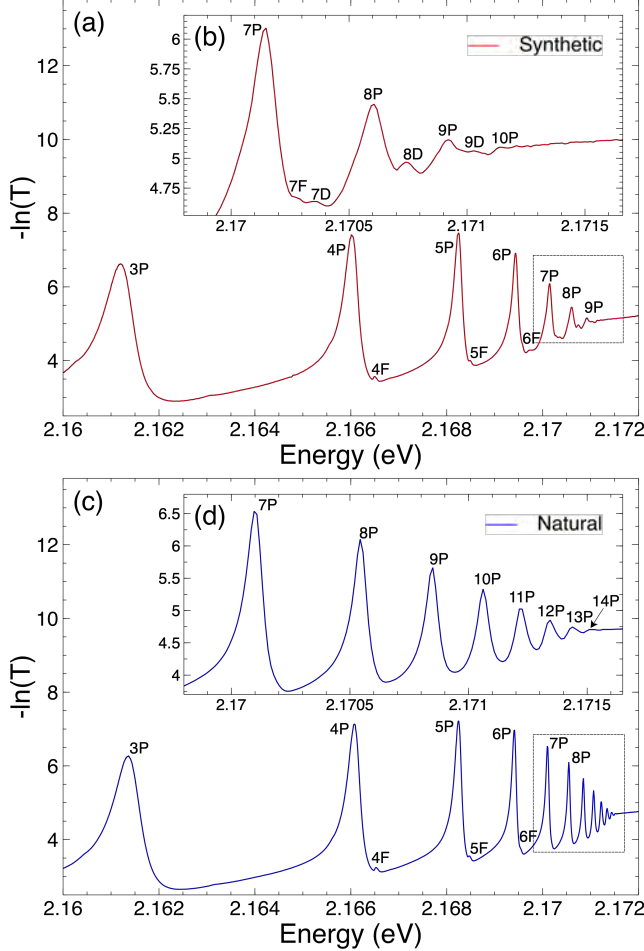

FIG. 3. Transmission spectrum for (a) synthetic (thickness 80 μm) and (c) natural (thickness 80 μm) samples of Cu_2O, measured at a nominal heat-sink temperature of 5 K. Insets (b) and (d) show the high-n regions delineated by boxes.

a Lumileds LXML-PX02 lime-green light emitting diode with emission wavelength centered at 565 nm, limited to 570-580 nm using an Omega optical 575BP10 band-pass filter, and the exciton spectra were recorded in transmission geometry. The excitation intensity was around $10 \, mW/cm^2$. Spectra were also recorded at lower excitation intensities to check that there were no power dependent effects. The spectra were obtained using a custom-made imaging spectrograph with a focal length of 1.9 m. The light was dispersed by a 1200 l/mm holographic grating of $(120 \times 140) \, mm^2$ size, 900 nm blaze wavelength, and detected by a CCD (Roper Pixis) of 1340×100 square pixels of 20 μm size. The spectromete has a resolution of 30 μeV (full width at half maximum (FWHM)) at 573 nm

(2.16 eV) in second order. Sample cooling was provided by a low-vibration closed-cycle cryostat (Montana Cryostation C2) equipped with a XYZ piezo stage (Attocube) that provided a spatial resolution around 0.1 μm, allowing focusing and lateral alignment.

A Rydberg series is clearly visible in both cases, extending to $n = 9$ (possibly $n = 10$) in the synthetic material, and $n = 14$ in the natural gemstone sample. These spectra show that our synthetic material is of high-quality, matching the highest principal quantum number previously observed for synthetic crystals [24]. However, exciton peaks above $n = 10$ are clearly missing. In both the natural and synthetic stones, from $n = 4$, we see small shoulders on the high energy flank of the P states. Due to their energy, and presence only for $n \geq 4$, we attribute these peaks to F states [41]. However, the synthetic sample shows additional peaks between the P and F peaks. By comparing the energy of these peaks to spectra measured through two-photon spectroscopy [42] we conclude these additional peaks are D states. The observation of D states in one-photon measurements is forbidden due to parity. However, if the crystal symmetry is broken, the selection rules are broken, and forbidden angular momentum states can be observed [43, 44]. Recent theoretical work has predicted that charged impurities in Cu_2O can cause the appearance of dipole-forbidden states and the disappearance of high n states [45]. In this work the authors consider charged impurity densities up to $10^{11} \, cm^{-3}$ which was shown to limit the Rydberg series to $n = 13$. We hypothesise that our crystal has a charged impurity density exceeding $10^{11} \, cm^{-3}$ causing our spectrum to be limited to $n = 10$.

In the remainder of this paper we investigate possible causes for the modified Rydberg spectrum. First we consider inhomogeneity due to strain before going on to search for point defects and vacancies impurities through photoluminescence (PL) and mid-infrared absorption (MIR) spectroscopy. We find that PL spectroscopy reveals a large quantity of copper vacancies which supports our hypothesis that charged impurities are perturbing the Rydberg spectrum.

Strain leads to shifts and splittings of the exciton energy levels [46]. If the strain is spatially inhomogeneous, then averaging, for example through the thickness of the sample, can cause broadening, with the eventual loss of visibility of higher-n peaks. By fitting the peaks in figure 3(a) with an asymmetric Lorentzian profile [47], we find that the energies of the P states are within 30 μeV of previously reported values [13]. Figure 4 shows the exciton spectra recorded at different positions along an approximately radial cross-section of the parent rod, at increments of ~ 100 μm. The overall structure of the exciton spectrum is remarkably uniform, with the additional peaks and the cut-off at high-n showing almost no variation across the sample. Close inspection of inset 4(c) reveals slight shifts in the energy of the exciton peaks, which we analyse in more detail in Fig. 5. Here we show the difference between the local energy of the $n = 6$ peak
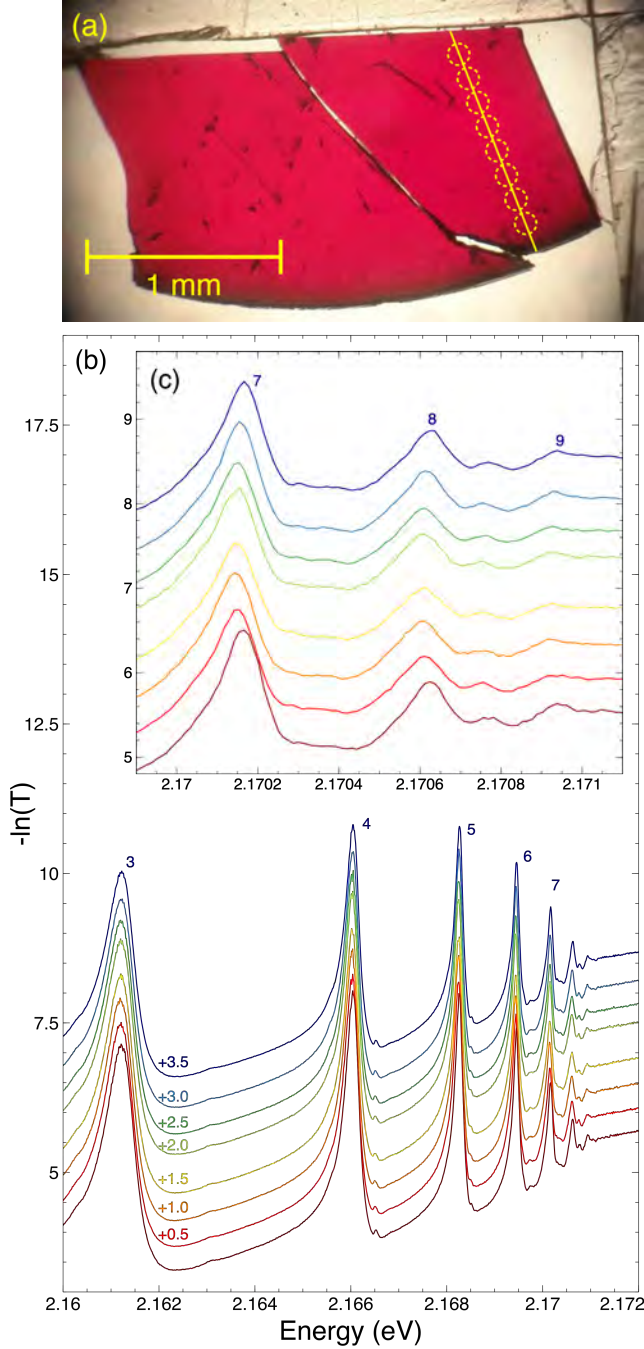
FIG. 4. (a) Low-magnification optical image of the synthetic Cu_2O sample, sandwiched between two CaF_2 cover-slips and confined by a spacer of slightly greater thickness than the sample. A small drop of glue that has leaked from the spacer anchors the bottom corner of piece of the sample on the right hand side. The left piece of the sample is mechanically free. (b) Spectral information extracted from different positions along the approximate radial cross-section of the parent rod indicated by the yellow dashed circles. Individual spectra have been offset by multiples of 0.5 to aid comparison. The inset (c) of this figure shows the same data on a magnified energy scale.

$E_6(r)$ and its whole sample mean value $\bar{E}_6$ as a function of position for both the synthetic and natural samples. The dispersion observed for the synthetic sample is significantly larger than for our best natural sample. Here the spread in $E_6(r)$ was 18.3 µeV for the natural sample, as compared to 103.9 µeV for the synthetic sample, measured over a similar scan range. Imaging of the samples through crossed polarisers qualitatively confirms there is some macroscopic strain in the synthetic material, the samples appeared similar to those shown in [48]. This indicates that local variation in the strain does occur, but given the similarity between the spectra in Fig. 4, this does not seem a plausible explanation for the observation of dipole-forbidden exciton states and the absence of higher-n states.
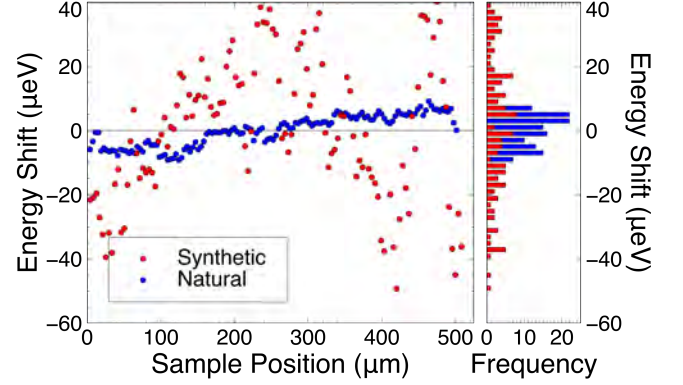

FIG. 5. Variation in the energy of the $n = 6$ peak for synthetic and natural samples, as a function of position across the sample. Here the spatial resolution was approximately 4.2 µm for the synthetic stone and 3.8 µm for the natural stone. On the right, histograms show the distribution of energy shift.

E. Photoluminescence Spectroscopy

Next we turn our attention to point defects, which we study using photoluminescence (PL) and mid-infrared absorption (MIR) spectroscopy. Figure 6 shows the PL spectrum measured at room temperature. Here the excitation source was a He:Ne laser operating at 543 nm. The excitation light was tightly focused onto the sample using a microscope objective with a numerical aperture of 0.6, which also served to collect the resulting luminescence. Residual excitation light was removed using a dichroic mirror, before the PL light was coupled into multi-mode optical fiber and guided to a wide-band grating spectrometer. The signals were carefully corrected for sample tilt and the chromatic aberration of the objective, enabling a quantitative comparison of the two samples across the full spectral range. The results are striking. For the natural sample, the dominant feature is due to quadrupole and phonon-assisted recombination of the 1S ortho-exciton. For the synthetic sample, this feature is drastically reduced, and instead the spectrum
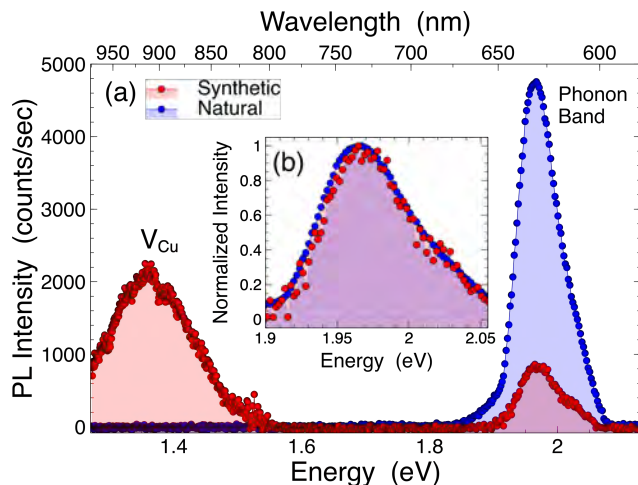
FIG. 6. (a) Broad-band photoluminescence (PL) spectrum recorded at room temperature for synthetic and natural gemstone samples. A broad emission peak associated with copper vacancies (V_{Cu}) dominates the PL emission in the synthetic sample at room temperature. Inset (b) the line-shape associated with the phonon emission band in both materials shows excellent agreement when normalized to the peak PL intensity as would be expected.

is dominated by below-gap luminescence at 1.4 eV which has previously been attributed to copper vacancies [39]. Note that at 300 K, oxygen vacancies are expected to be ionized [49], and we do not see their luminescence at 1.70 eV in either sample.

To investigate these effects with higher resolution, we also performed PL measurement at low temperature using the same high-resolution spectrometer as in figure 3. For these measurements, the input slit aperture was 20 µm, corresponding to 1.16 µm at the sample plane. The corresponding spectral resolution is 70 µeV at 611 nm (2.01 eV) in first order. The Cu_2O was illuminated by above band gap continuous-wave low-intensity radiation ($\approx$ 50 µW) with wavelength $\lambda = 532$ nm. We performed a high-resolution study of the region near the band edge (Fig. 7(b)), as well as localized measurements at energies associated with oxygen and copper vacancies (Fig. 7(a)). The influence of excitation intensity on line-shape was investigated and found to be negligible. The main effect that we observed was that the temperature of the excitons increased marginally at higher excitation intensity.

The region close to the band edge shows good agreement with a previous PL studies [51, 52]. The intense sharp peak at $\sim$ 2.03 eV is direct emission from the 1S ortho-exciton line. Very similar characteristics defined this spectral line in both materials. The best fit was achieved using a pseudo-Voigt profile superimposed on the exponential Bose-Einstein tail of the first phonon replica. In both materials the line exhibited a similar asymmetry in the tails of the profile. This asymmetry is highlighted for the synthetic material in the inset

Fig. 7(d). The line fits gave a center value of 2.0328 eV for the peak and full width of 127 µeV for the synthetic material, and a center value of 2.0327 eV for the peak and full width of 135 µeV for the gemstone material. These line-widths are above our calibrated resolution limit of 70 µeV at 611 nm, and probably reflect the inhomogeneous broadening due to strain discussed earlier. The position of the 1S ortho-exciton line is roughly 700 µeV from previously reported values [53]. As the shift is almost the same for both the natural and synthetic stones we attribute this to a systematic error in the calibration. The other large peaks in the range 1.950–2.025 eV are phonon replicas of the main 1S ortho-exciton line [51]. The line-shape of these peaks can be fitted with the convolution of two terms describing the exciton density of states (DoS) and thermal occupation statistics respectively [54]. The low-energy side has a rising edge, which scales with the 3D DoS, $g^{3D}(E)$. The high-energy side has an exponential tail from the exciton Bose-Einstein population statistics, which can be approximated to the Boltzmann distribution $f_B(E)$, since the exciton gas is of low-density. The PL intensity $I_{PL} \propto g^{3D}(E)f_B(E)$ is then described by,

$$I_{PL} = A(E - E_0)^{1/2} \exp\left[-\frac{(E - E_0)}{k_B T}\right] \ , \qquad (3)$$

where A is a proportionality constant and E_0 is the energy of the exciton at zero momentum minus the phonon energy, the latter assumed to be dispersion-less. A similar line-shape fitting function was used in [51, 52]. The fitting function gave a temperature of $\sim$ 13 K and $\sim$ 10 K for the exciton gases in the synthetic and natural samples respectively. This is in acceptable agreement with the nominal heat-sink temperature of 5 K, because the exciton gas is expected to be at a slightly higher temperature than the crystal lattice [55]. Table I shows the energies obtained from the fitted spectral line-shapes of several of the exciton phonon replicas, as well as the values reported in [51] for comparison. A theoretical phonon spectrum in Cu_2O can be found in [56] and is in good agreement with the values presented in Table I. We have not reported the energies of the Γ_5^- and $\Gamma_4^{-(1)}$(LO) phonon assisted transitions in this table because we are not confident that they can be reliably deconvolved from the dominant neighbouring phonon assisted transitions in our PL data. The agreement with the values reported in [51] is otherwise excellent. We have, however, observed some differences between our natural gemstone PL spectrum and the data presented by the Kyoto group [51]. The PL spectrum in their paper shows a sharp peak located at 1.947 eV, which sits on the red-shifted shoulder of the double-peaked phonon feature above just 1.95 eV. We see no evidence of this spectral feature in our PL spectrum. In contrast, we observe two small sharp peaks at 1.914 eV and 1.916 eV, which are not present in [51]. These two peaks have been observed in previous PL studies [52, 57] but have not been assigned. Unfortunately, the signal-to-noise ratio for our synthetic Cu_2O PL spectrum is in-
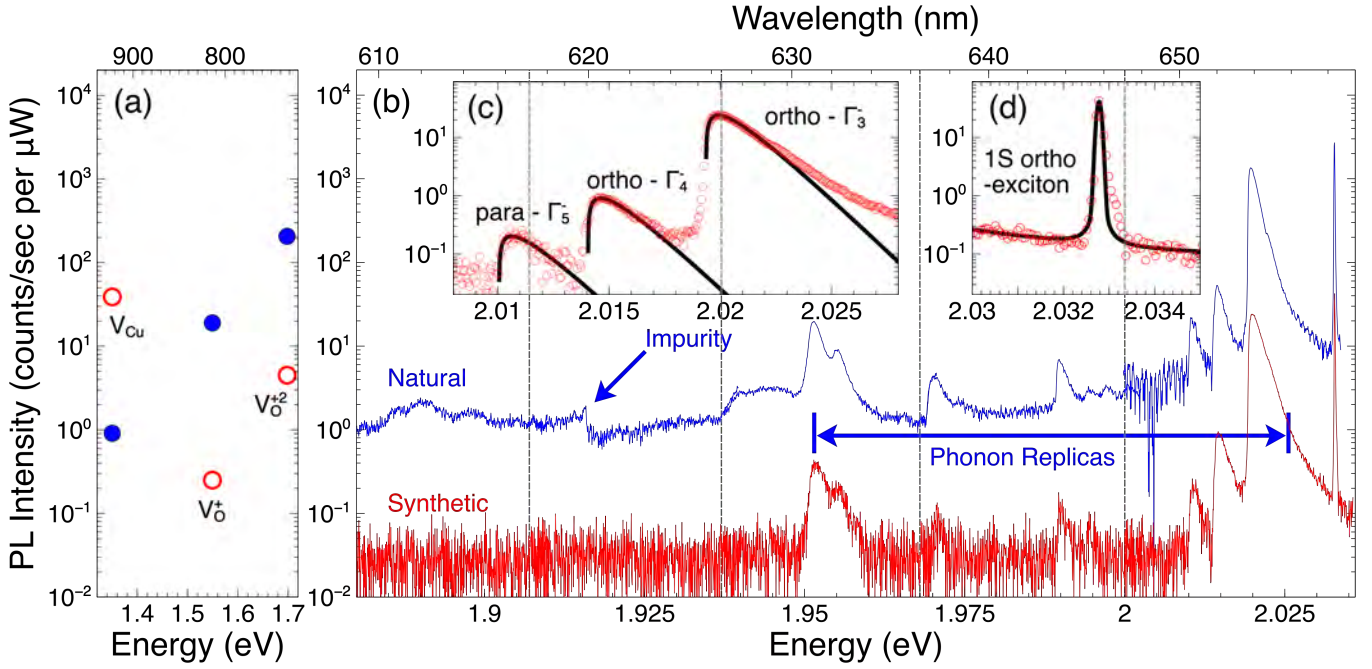
FIG. 7. High-resolution photoluminescence (PL) spectra recorded at low temperature (≈ 5 K) for synthetic (red) and natural gemstone (blue) Cu_2O normalised with respect to pump power. The subsidiary figure (a) shows the infrared PL intensity at three discrete emission wavelengths (918 nm, 800 nm, and 730 nm) associated with Cu and O vacancies, and assigned according to [50]. The main figure (b) shows the visible PL in the range 609-659 nm. The insets in this figure show (c) three phonon replicas for the synthetic material on an expanded energy scale fitted (black line) to equation 3, and (d) the ortho-phonon line fitted (black line) with a pseudo-Voigt profile also on an expanded energy scale. The lines have been assigned according to [51]. The photoluminescence was much brighter for the natural gemstone, which accounts for the signal-to-noise improvement. Two small peaks not associated with phonons were observed in the natural gemstone PL spectrum at 1.914 eV (647.8 nm) and 1.916 eV (647.1 nm) which we attribute to impurity luminescence.

TABLE I. Energy positions of the phonon assisted lines (in eV). The relative positions with respect to the resonance energy of the yellow 1S ortho-exciton are also tabulated (in meV) and compared with the values reported in [51].

Phonon	Center (eV)	This work (meV)	[51] (meV)
Γ_5^-			10.5
Γ_3^-	2.0192	13.6	13.5
$\Gamma_4^{-(1)}$(TO)	2.0140	18.8	18.8
$\Gamma_4^{-(1)}$(LO)			19.3
Γ_2^-	1.9892	43.6	43.4
Γ_5^+	1.9693	63.5	63.2
$\Gamma_4^{-(2)}$(TO)	1.9543	78.5	78.4
$\Gamma_4^{-(2)}$(LO)	1.9507	82.1	82.0

sufficient to resolve these spectral features. We speculate that the origin of these peaks is due to different trace impurities to those found in the Kyoto samples. We have also recorded the intensity of the PL emission at three discrete wavelengths known to be associated with copper and oxygen vacancies [48, 50] in both synthetic and natural samples (Fig. 7(a)). Measurements at 1.35 eV (918 nm) confirm the observation of strong luminescence from copper vacancies observed in the room temperature spectrum. Measurements at 1.70 eV (800 nm) and 1.55 eV (730 nm) and are associated with singly and doubly ionized oxygen vacancies, V_O^{+1} and V_O^{+2}, respectively [50]. These peaks are not observed in the room temperature data. Here we find that the luminescence from these states is strongest in the natural sample.

In summary, the region close to the band edge indicates a narrow 1S exciton and all the expected phonon modes in both samples. Apart from the stronger overall luminescence of the natural sample at low temperature, the spectrum of the two samples is largely identical in this region. However, the PL measurements indicate a large excess of copper vacancies in the synthetic material, which has been shown to be the result of the fabrication process (oxidation of the copper rod) [38]. We believe the copper vacancies are responsible for limiting the Rydberg series to $n = 10$ [45].

F. Mid-Infrared Spectroscopy

To search for other impurities that might alter the Rydberg spectrum, we also performed MIR measurements

to look for shallow bound states such as those observed in silicon [58]. Much like excitons, impurity states are good sensors of the local crystal environment around the defect, and their inhomogeneous line-width is another indicator of the material quality [59]. There is little information in the literature about the mid- and far-infrared properties of single crystal Cu_2O. A transmission spectrum for a 39.8 μm thin film was reported in [60], although many of the spectral features are obscured by Fabry-Perot interference fringes. The spectra in this work were recorded using a Bruker Vertex 80V Fourier transform spectrometer (FTS). The samples were mounted on the cold-finger of a helium flow cryostat located in the spectrometer absorption compartment, and the optical path within the spectrometer was fully evacuated. Sample illumination was provided by the internal FTS globar, and the transmitted interferogram was recorded on a liquid nitrogen cooled mercury cadmium telluride (MCT) detector. Cooling was provided by a closed-cycle ColdEdge™ "Stinger" helium re-circulator.

Figure 8 shows the mid-infrared transmission spectrum for both (a) synthetic and (c) natural samples recorded for a range of temperatures between 8 K and 300 K. The samples exhibited very similar spectra with only some minor differences. The spectra are dominated by two Reststrahlen bands between 95-115 meV and 135-155 meV. Some additional peaks become more visible when the y-axis is expanded as shown in the inset. The shoulder at 164 meV relates to the second Reststrahlen band and is present in both samples. In both cases this shoulder sharpens to a discernible peak at lower temperatures. We attribute this peak to the highest energy longitudinal optical (LO) phonon. The peak at 205 meV is also present in both samples. This peak shows a weak temperature dependence, becoming slightly sharper at lower temperature. While also present in both samples, a second peak at 215 meV appears stronger in the natural sample. The physical origin of these spectral features is open to debate. It is generally accepted that synthetically grown Cu_2O is always p-type [61], and acceptor levels due to copper vacancies lying at 220 meV and 470 meV have been proposed. Previous density functional theory (DFT) calculations performed by the same research group [62] pointed towards a hole trap 450 meV above the valence band edge attributed to single copper vacancies, and a second hole trap around 250 meV tentatively attributed to a copper di-vacancies. We do not observe the 450 meV feature in either sample but the peaks we observe at 205 meV and 215 meV could fit either the copper vacancy or di-vacancy prediction. There is also some experimental evidence to support this hypothesis [63]. Two hole trap levels consistent with this description have been observed in the deep level transient spectrum (DLTS) of polycrystalline p-type Cu_2O epilayers grown on top of intrinsic zinc oxide (i-ZnO) and fabricated into mesa heterostructures. Theoretical calculations exploiting the generalized gradient approximation to DFT have also been used to predict a single copper
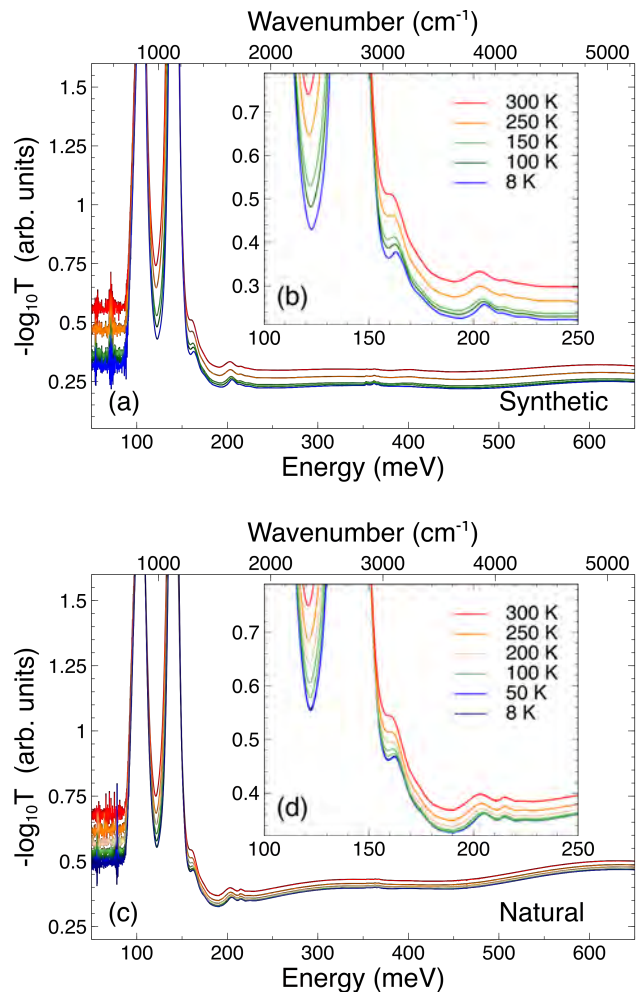

FIG. 8. (a) MIR transmission spectra of a 1 mm thick slice of synthetic Cu_2O crystal recorded at various temperatures between 8 K and 300 K. The sample was wedged at an angle of 1° to avoid Fabry-Perot fringing. The transmission T here is the ratio of the ratio of the signal on the MCT detector with and without the sample, i.e. $T = I/I_0$. The increased noise below 80 meV indicates where the MCT detector response falls off at long wavelengths. The inset (b) shows the long-wavelength region near the Reststrahlen band edge on an expanded energy scale. (c) MIR transmission spectra of a similarly wedged 1 mm thick slice of natural Cu_2O gemstone acquired at a location where high-n excitons were observed and measured under similar conditions. The inset (d) similarly shows the region near the Reststrahlen band edge on an expanded energy scale.

vacancy level at 280 meV in p-type Cu_2O [64]. Another possibility is that this feature could be associated with multi-phonon absorption. The spectral location matches twice the energy of the observed phonon bands, and the fact that the spectral feature is observed in two samples of completely different origin strongly suggests that it is intrinsic to the material. Multi-phonon processes have previously been observed in PL spectroscopy [51, 52].

III. CONCLUSIONS

In summary, there are strong similarities between the excitonic spectrum that we observe in the synthetic material and that observed in high-quality natural gemstones. The principal differences are a cut-off at lower principal quantum number, the emergence of dipole-forbidden peaks, and an overall shift in the spectrum. We note however that the observation of $n = 10$ in synthetic material is comparable to the state-of-the-art [24]. The large spatial extent of the high-n exciton wave-functions means that they are sensitive to lattice imperfections. For example, using the formula for the Bohr radius of the P-exciton series quoted in [13], together with $a_B = 1.11$ nm, would give $\langle r_{10} \rangle = 165$ nm, which corresponds to 386 lattice constants. Measurements of the 1S ortho-exciton width and the spatial variation of the Rydberg spectrum suggest that inhomogeneous strain cannot explain the origin of these features. We know that inhomogeneous strain fields are present in the synthetic material because we have performed some basic experiments. See Supplemental Material at [65] for a description of the experiments performed to assess the strain using crossed polarisers [66], and spatial mapping of the spectral properties associated with the $n = 6$ exciton line. PL measurements demonstrate a large excess of copper vacancies as well as the quenching of the band-edge luminescence associated with intrinsic effects in the synthetic sample. A search for additional shallow donor states in the MIR region did not produce a clear result. Our observations of an excess of copper vacancies and a modified Rydberg spectrum are in good qualitative agreement with theoretical work [45], and so we postulate that the presence of the copper vacancies is causing the changes to the Rydberg spectrum. In order for the Rydberg series to be limited to $n = 10$ the density of the copper vacancies must exceed 10^{11} cm^{-3}, which was the highest density considered in [45]. We have not attempted to address these problems yet, but there are many promising post-growth treatments to try. For example, annealing at high-temperature has been successfully employed to remove the CuO-walled voids [24, 37] and reduce the concentration of copper vacancies [38, 67]. The mechanical polishing procedure employed to produce samples for optical experiments may itself introduce problems that are specific to the sample origin. In the synthetic material, mechanical polishing can open some of the CuO-walled voids and this can deposit unspecified material into the polishing slurry. We have on occasion observed the appearance of new scratches and micro-cracking of the surface during the polishing process when this happens. However, there are fabrication strategies such as chemical etching [51] or ion-beam milling that might mitigate the consequences of this type of surface damage.

Our results are important because they demonstrate that it is possible to produce large scale bulk synthetic material with comparable optical properties to natural gemstone material. This represents a significant step forward because it shows that there is a viable technological route towards harnessing the quantum optical properties of this extraordinary semiconductor material.

[1] N. Šibalić and C. S. Adams, *Rydberg Physics*, 2399-2891 (IOP Publishing, 2018).

[2] D. H. Meyer, Z. A. Castillo, K. C. Cox, and P. D. Kunz, Assessment of Rydberg atoms for wideband electric field sensing, Journal of Physics B: Atomic, Molecular and Optical Physics **53**, 034001 (2020).

[3] A. Browaeys and T. Lahaye, Many-body physics with individually controlled Rydberg atoms, Nature Physics , 1 (2020).

[4] M. Saffman, Quantum computing with atomic qubits and Rydberg interactions: progress and challenges, Journal of Physics B: Atomic, Molecular and Optical Physics **49**, 202001 (2016).

[5] O. Firstenberg, C. S. Adams, and S. Hofferberth, Nonlinear quantum optics mediated by Rydberg interactions, Journal of Physics B: Atomic, Molecular and Optical Physics **49**, 152003 (2016).

[6] L. O. Grondahl and P. H. Geiger, A new electronic rectifier, Journal of the A.I.E.E. **46**, 215 (1927).

[7] L. O. Grondahl, The copper-cuprous-oxide rectifier and photoelectric cell, Rev. Mod. Phys. **5**, 141 (1933).

[8] L.-C. Chen, Review of preparation and optoelectronic characteristics of Cu_2O-based solar cells with nanostructure, Materials Science in Semiconductor Processing **16**, 1172 (2013), Advanced Oxides for Electronics.

[9] E. F. Gross, Optical spectrum of excitons in the crystal

lattice, Il Nuovo Cimento (1955-1965) **3**, 672 (1956).

[10] C. Weisbuch, H. Benisty, and R. Houdré, Overview of fundamentals and applications of electrons, excitons and photons in confined structures, Journal of Luminescence **85**, 271 (2000).

[11] P. W. Baumeister, Optical absorption of cuprous oxide, Phys. Rev. **121**, 359 (1961).

[12] D. Snoke and G. M. Kavoulakis, Bose–Einstein condensation of excitons in Cu_2O: progress over 30 years, Reports on Progress in Physics **77**, 116501 (2014).

[13] T. Kazimierczuk, D. Fröhlich, S. Scheel, H. Stolz, and M. Bayer, Giant Rydberg excitons in the copper oxide Cu_2O, Nature **514**, 343 (2014).

[14] D. L. Dexter and R. S. Knox, *Excitons*, Interscience Tracts on Physics and Astronomy, Vol. 25 (New York: Interscience Publishers, 1965).

[15] A. M. Fox, *Optical Properties of Solids*, Oxford Master Series in Condensed Matter Physics (Oxford University Press, 2003).

[16] J. W. Hodby, T. E. Jenkins, C. Schwab, H. Tamura, and D. Trivich, Cyclotron resonance of electrons and of holes in cuprous oxide, Cu_2O, Journal of Physics C: Solid State Physics **9**, 1429 (1976).

[17] N. Naka, I. Akimoto, M. Shirai, and K.-i. Kan'no, Time-resolved cyclotron resonance in cuprous oxide, Phys. Rev. B **85**, 035209 (2012).

[18] G. M. Kavoulakis, Y.-C. Chang, and G. Baym, Fine structure of excitons in Cu_2O, Phys. Rev. B **55**, 7593 (1997).

[19] V. Walther, S. O. Krüger, S. Scheel, and T. Pohl, Interactions between Rydberg excitons in Cu_2O, Phys. Rev. B **98**, 165201 (2018).

[20] H. Busche, P. Huillery, S. W. Ball, T. Ilieva, M. P. A. Jones, and C. S. Adams, Contactless nonlinear optics mediated by long-range Rydberg interactions, Nature Physics **13**, 655 (2017).

[21] M. D. Lukin, M. Fleischhauer, R. Cote, L. M. Duan, D. Jaksch, J. I. Cirac, and P. Zoller, Dipole blockade and quantum information processing in mesoscopic atomic ensembles, Phys. Rev. Lett. **87**, 037901 (2001).

[22] J. D. Pritchard, D. Maxwell, A. Gauguet, K. J. Weatherill, M. P. A. Jones, and C. S. Adams, Cooperative atom-light interaction in a blockaded Rydberg ensemble, Phys. Rev. Lett. **105**, 193603 (2010).

[23] J. Heckötter, M. Freitag, D. Fröhlich, M. Aßmann, M. Bayer, P. Grünwald, F. Schöne, D. Semkat, H. Stolz, and S. Scheel, Rydberg excitons in the presence of an ultralow-density electron-hole plasma, Phys. Rev. Lett. **121**, 097401 (2018).

[24] T. Ito, H. Yamaguchi, K. Okabe, and T. Masumi, Single-crystal growth and characterization of Cu_2O and CuO, Journal of Materials Science **33**, 3555 (1998).

[25] M. Khazali, K. Heshami, and C. Simon, Single-photon source based on Rydberg exciton blockade, Journal of Physics B: Atomic, Molecular and Optical Physics **50**, 215301 (2017).

[26] V. Walther, R. Johne, and T. Pohl, Giant optical nonlinearities from Rydberg excitons in semiconductor microcavities, Nature Communications **9**, 10.1038/s41467-018-03742-7 (2018).

[27] S. Zielińska-Raczyńska, G. Czajkowski, K. Karpiński, and D. Ziemkiewicz, Nonlinear optical properties and self-kerr effect of Rydberg excitons, Phys. Rev. B **99**, 245206 (2019).

[28] V. Walther, P. Grünwald, and T. Pohl, Controlling exciton-phonon interactions via electromagnetically induced transparency, Phys. Rev. Lett. **125**, 173601 (2020).

[29] S. B. Ogale, P. G. Bilurkar, N. Mate, S. M. Kanetkar, N. Parikh, and B. Patnaik, Deposition of copper oxide thin films on different substrates by pulsed excimer laser ablation, Journal of Applied Physics **72**, 3765 (1992).

[30] A. O. Musa, T. Akomolafe, and M. J. Carter, Production of cuprous oxide, a solar cell material, by thermal oxidation and a study of its physical and electrical properties, Solar Energy Materials and Solar Cells **51**, 305 (1998).

[31] K. Santra, P. Chatterjee, and S. P. S. Gupta, Powder profile studies in electrodeposited cuprous oxide films, Solar Energy Materials and Solar Cells **57**, 345 (1999).

[32] A. K. Mukhopadhyay, A. K. Chakraborty, A. P. Chatterjee, and S. K. Lahiri, Galvanostatic deposition and electrical characterization of cuprous oxide thin films, Thin Solid Films **209**, 92 (1992).

[33] N. Naka, S. Hashimoto, and T. Ishihara, Thin films of single-crystal cuprous oxide grown from the melt, Japanese Journal of Applied Physics **44**, 5096 (2005).

[34] S. Jeong and E. S. Aydil, Heteroepitaxial growth of Cu_2O thin film on ZnO by metal organic chemical vapor deposition, Journal of Crystal Growth **311**, 4188 (2009).

[35] V. T. Agekyan, Spectroscopic properties of semiconductor crystals with direct forbidden energy gap, Physica Status Solidi (a) **43**, 11 (1977).

[36] S. O. Krüger and S. Scheel, Waveguides for rydberg excitons in Cu_2O from strain traps, Phys. Rev. B **97**, 205208 (2018).

[37] R. D. Schmidt-Whitley, M. Martinez-Clemente, and A. Revcolevschi, Growth and microstructural control of single crystal cuprous oxide Cu_2O, Journal of Crystal Growth **23**, 113 (1974).

[38] K. B. Chang, L. Frazer, J. J. Schwartz, J. B. Ketterson, and K. R. Poeppelmeier, Removal of copper vacancies in cuprous oxide single crystals grown by the floating zone method, Crystal Growth & Design **13**, 4914 (2013).

[39] L. Frazer, K. B. Chang, K. R. Poeppelmeier, and J. B. Ketterson, Cupric oxide inclusions in cuprous oxide crystals grown by the floating zone method, Science and Technology of Advanced Materials **16**, 034901 (2015).

[40] B. K. Meyer, A. Polity, D. Reppin, M. Becker, P. Hering, B. Kramm, P. J. Klar, T. Sander, C. Reindl, C. Heiliger, M. Heinemann, C. Müller, and C. Ronning, Chapter six - the physics of copper oxide (Cu_2O), in *Oxide Semiconductors*, Semiconductors and Semimetals, Vol. 88, edited by B. G. Svensson, S. J. Pearton, and C. Jagadish (Elsevier, 2013) pp. 201 – 226.

[41] J. Thewes, J. Heckötter, T. Kazimierczuk, M. Aßmann, D. Fröhlich, M. Bayer, M. A. Semina, and M. M. Glazov, Observation of high angular momentum excitons in cuprous oxide, Phys. Rev. Lett. **115**, 027402 (2015).

[42] J. Mund, D. Fröhlich, D. R. Yakovlev, and M. Bayer, High-resolution second harmonic generation spectroscopy with femtosecond laser pulses on excitons in Cu_2O, Phys. Rev. B **98**, 085203 (2018).

[43] J. Heckötter, M. Freitag, D. Fröhlich, M. Aßmann, M. Bayer, M. A. Semina, and M. M. Glazov, Scaling laws of Rydberg excitons, Phys. Rev. B **96**, 125142 (2017).

[44] J. Heckötter, M. Freitag, D. Fröhlich, M. Aßmann, M. Bayer, M. A. Semina, and M. M. Glazov, Influence of the wavefunction distribution on exciton dissociation in electric field, Physics of the Solid State **60**, 1506 (2018).

[45] S. O. Krüger, H. Stolz, and S. Scheel, Interaction of charged impurities and rydberg excitons in cuprous oxide, Phys. Rev. B **101**, 235204 (2020).

[46] H. R. Trebin, H. Z. Cummins, and J. L. Birman, Excitons in cuprous oxide under uniaxial stress, Phys. Rev. B **23**, 597 (1981).

[47] Y. Toyozawa, Theory of line-shapes of the exciton absorption bands, Progress of Theoretical Physics **20**, 53 (1958).

[48] L. Frazer, E. J. Lenferink, K. B. Chang, K. R. Poeppelmeier, N. P. Stern, and J. B. Ketterson, Evaluation of defects in cuprous oxide through exciton luminescence imaging, Journal of Luminescence **159**, 294 (2015).

[49] S. Koirala, N. Naka, and K. Tanaka, Correlated lifetimes of free paraexcitons and excitons trapped at oxygen vacancies in cuprous oxide, Journal of Luminescence **134**, 524 (2013).

[50] L. Frazer, K. B. Chang, R. D. Schaller, K. R. Poeppelmeier, and J. B. Ketterson, Vacancy relaxation in cuprous oxide ($Cu_{2-x}O_{1-y}$), Journal of Luminescence **183**, 281 (2017).

[51] M. Takahata and N. Naka, Photoluminescence properties of the entire excitonic series in Cu_2O, Phys. Rev. B **98**, 195205 (2018).

[52] Y. Petroff, P. Y. Yu, and Y. R. Shen, Study of photoluminescence in cu₂o, Phys. Rev. B **12**, 2488 (1975).

[53] L. Frazer, K. B. Chang, K. R. Poeppelmeier, and J. B. Ketterson, Photoionization cross section of $1s$ orthoexcitons in cuprous oxide, Phys. Rev. B **89**, 245203 (2014).

[54] R. J. Elliott, Intensity of optical absorption by excitons, Physical Review **108**, 1384 (1957).

[55] J. P. Wolfe and J. I. Jang, The search for bose–einstein condensation of excitons in Cu_2O: exciton-auger recombination versus biexciton formation, New Journal of Physics **16**, 123048 (2014).

[56] P. A. Korzhavyi and B. Johansson, *Literature review on the properties of cuprous oxide Cu_2O and the process of copper oxidation*, Tech. Rep. SKB TR-11-08 (Department of Materials Science and Engineering, Royal Institute of Technology, Stockholm., 2011).

[57] K. E. O'Hara, *Relaxation kinetics of excitons in cuprous oxide*, Ph.D. thesis, University of Illinois (1999).

[58] C. Jagannath, Z. W. Grabowski, and A. K. Ramdas, Linewidths of the electronic spectra of donors in silicon, Phys. Rev. B **23**, 2082 (1981).

[59] S. A. Lynch, G. Matmon, S. G. Pavlov, K. L. Litvinenko, B. Redlich, A. F. G. van der Meer, N. V. Abrosimov, and H.-W. Hübers, Inhomogeneous broadening of phosphorus donor lines in the far-infrared spectra of single-crystalline SiGe, Phys. Rev. B **82**, 245206 (2010).

[60] M. O'Keeffe, Infrared optical properties of cuprous oxide, The Journal of Chemical Physics **39**, 1789 (1963).

[61] D. O. Scanlon and G. W. Watson, Undoped n-type Cu_2O: Fact or fiction?, The Journal of Physical Chemistry Letters **1**, 2582 (2010).

[62] D. O. Scanlon, B. J. Morgan, G. W. Watson, and A. Walsh, Acceptor levels in p-type Cu_2O: Rationalizing theory and experiment, Phys. Rev. Lett. **103**, 096405 (2009).

[63] G. K. Paul, Y. Nawa, H. Sato, T. Sakurai, and K. Akimoto, Defects in Cu_2O studied by deep level transient spectroscopy, Applied Physics Letters **88**, 141901 (2006).

[64] H. Raebiger, S. Lany, and A. Zunger, Origins of the p-type nature and cation deficiency in Cu_2O and related materials, Phys. Rev. B **76**, 045209 (2007).

[65] *URL will be inserted by publisher*.

[66] A. S. Redner, Nondestructive evaluation using polarized light, Materials Evaluation **53**, 642 (1995).

[67] R. G. Kaufman and R. T. Hawkins, Annealing of copper and oxygen vacancies in cuprous oxide films monitored by low temperature luminescence, Journal of The Electrochemical Society **133**, 2652 (1986).